

# ME 502 Project Report

## Project #5 – Evaporator in Wet Condition

Jiong Chen

### 1. Abstract

In this project, the heat transfer and hydrodynamics of an evaporator is analyzed by applying finite volume concept. The evaporator is a flat-tube-and-fin heat exchanger with two slab and the arrangement is counter-flow and cross-flow. The profile of important parameters such as temperature, pressure and HTC along the tube of the heat exchanger is studied. A simplified condensation model is applied, and the results shows that increasing relative humidity can increase HTC of refrigerant and for higher air volumetric flow rate, the HTC of refrigerant is increased.

### 2. Introduction

A cooling coil, also known as an evaporator coil, is a key component of an air conditioning system. It is responsible for removing heat and moisture from the air that is circulated through the system. Cooling coils are typically made of copper or aluminum tubes that are surrounded by a series of thin metal fins, which increase the surface area and improve heat transfer. The coils contain a refrigerant, which is a chemical that absorbs heat from the air as it passes over the coils, causing the refrigerant to evaporate. This process cools the air and removes moisture, which is then drained away. Cooling coils are crucial to the proper functioning of an air conditioning system, and proper maintenance and cleaning is essential to ensure their longevity and efficiency.

In this work, python code with CoolProp package is used to simulate the evaporator given the geometry and operating conditions of the evaporator. A simplified condensation model is applied in the program when the surface temperature is lower than the dew point temperature. First, with the given operating condition, the overall performance of the evaporator is predicted. Then different relative humidity and was applied to investigate the impact to the performance of the evaporator.

### 3. Methods and Assumptions

#### 3.1 Geometries and Operation Conditions

The operating fluid is R1234yf. The subcooled refrigerant exists the condenser of the air-conditioning unit. It is reasonable to assume that  $h_{cro} = h_{eri}$ . The humid air stream and the refrigerant stream are in a cross-flow and counter-flow arrangement. The detailed geometry and operation conditions of the evaporator are listed in Table 1-3.

Table 1. Dimensions of the tubes of the cooling coil

Tube Geometry	Size
N_slab: number of slabs (rows), [-]	4
N_pass: number of passes in one slab, [-]	1
L_tube_pass: tube length in one pass, [mm]	300
N_tube_pass: number of tubes in one pass, [-]	25
t_wall*: wall thickness, [mm]	0.35
t_tube: tube thickness, [mm]	1.7
D_tube: tube depth, tube major, [mm]	10
n_port: number of ports in one tube, [-]	7

<b>Ra_tube: roughness of tube inner surface, [m]</b>	$10^{-6}$
--	-----------

\* t<sub>wall</sub>: assume all the outer walls and inner walls have the same thickness.

Table 2. Dimensions of the fins of the cooling coil

Fin Geometry	Size
<b>theta_louver: louver angle, [deg]</b>	15
<b>P_louver: louver pitch, [mm]</b>	1.3
<b>L_louver: louver length, [mm]</b>	7.2
<b>N_louverbank: number of louver sets per fin [-]</b>	2
<b>h_fin: fin height, [mm]</b>	8
<b>t_fin: fin thickness, [mm]</b>	0.1
<b>P_fin: fin pitch, [mm]</b>	1.8 (14 FPI*)
<b>D_fin: fin depth, [mm]</b>	10

\* FPI: fin per inch

Table 3. Operating Conditions

Parameter	Value
<b>T_cro: condenser outlet temperature, [°C]</b>	40
<b>P_cro: condenser outlet pressure, [kPaA]</b>	1250
<b>h_eri: refrigerant inlet specific enthalpy, [kJ/kg]</b>	$h_{eri} = h_{cro}$
<b>m_dot_er: refrigerant mass flow rate, [g/s]</b>	35
<b>SH_ero: refrigerant superheat at the outlet, [°C]</b>	8
<b>T_eai: air inlet temperature, [°C]</b>	35
<b>P_eai: air inlet pressure, [kPaA]</b>	99.5
<b>m_dot_eai: air inlet mass flow rate, [kg/min]</b>	9

The schematic of the evaporator is shown in Figure 1. Assumptions were made - uniform distribution of refrigerant and air flow. Thus, only one tube calculation is needed. The tube will be divided into “n” small segments. Due to cross-flow counter-flow arrangement, calculation will start from the outlet of the evaporator. The output of the current element will be the input condition of the next element.

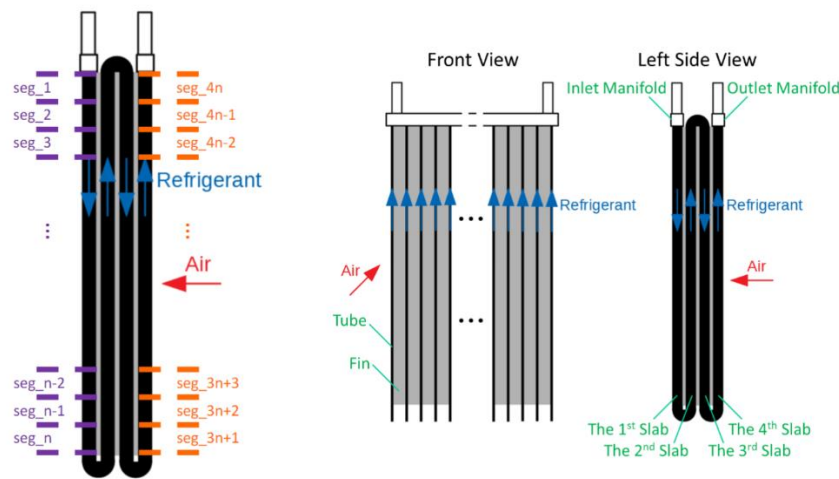


Figure 1. Schematic of evaporator

### 3.2 Simplified Condensation Model

In the program, air is humid air, so condensation could happen. A simplified condensation model is applied. The schematic of the simplified condensation model is shown in Figure 2. The key assumptions of this model are: the temperature of water-EG-side surface of the wall  $T_{s,eg}$  is uniform; the convection heat transfer coefficient  $HTC_{eg}$  is constant. The air side heat transfer rate is composed of latent heat transfer rate and sensible heat transfer rate.

The sensible heat transfer rate can be calculated by:

$$T_{a,o} = T_{s,a} + (T_{a,i} - T_{s,a}) \exp\left(-\frac{HTC_a A_{s,a}}{\dot{m}_a c_{p,a}}\right)$$

$$Q_{a,sen} = \dot{m}_a c_{p,a} (T_{a,i} - T_{a,o})$$

The latent heat transfer rate can be obtained by analogy of sensible heat transfer rate:

$$MTC_a = \frac{HTC_a}{\rho_a c_{p,a} Le_a^{1-n}}, Le_a = \frac{\alpha_a}{D_{AB,a}}, D_{AB,a} = 0.26 \times 10^{-4} m^2/s, n = \frac{1}{3}$$

$$\rho_{A,o} = \rho_{A,s} + (\rho_{A,i} - \rho_{A,s}) \exp\left(-\frac{MTC_a A_{s,a}}{\dot{V}_a}\right)$$

$$\omega_{a,o} = \frac{\rho_{A,o}}{\rho_{da,o}} = \frac{\rho_{A,o}}{\rho_{da,i}} = \rho_{A,o} v_{da,i}$$

$$\dot{m}_{condensate} = \dot{m}_{da} (\omega_{a,i} - \omega_{a,o})$$

$$Q_{a,lat} = \dot{m}_{condensate} h_{fg}$$

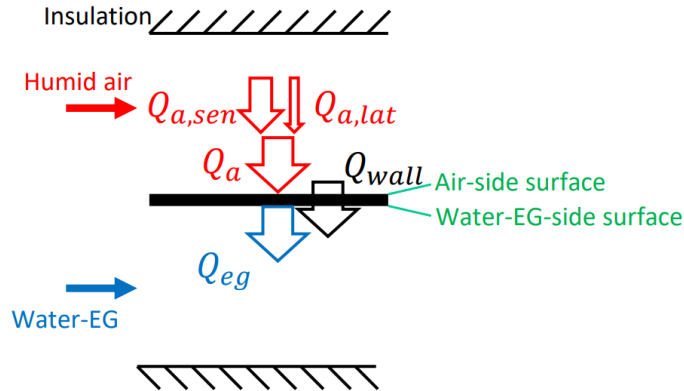


Figure 2. Schematic of simplified condensation model

From the schematic of simplified condensation model, the fin geometry is simplified to a plane-tube wall. However, when calculating the air-side surface area, the overall surface efficiency can be applied for the sensible heat transfer calculation; and for latent heat transfer calculation, the overall surface efficiency for mass transfer can be approximated as  $\eta_{o,m} = \eta_o^{0.5}$ .

EG side heat transfer rate can be calculated:

$$T_{eg,o} = T_{s,a} - (T_{s,a} - T_{eg,i}) \exp \left( - \frac{1}{\dot{m}_{eg} c_{p,eg} [R_{wall} + 1/(HTC_{eg} A_{s,eg})]} \right)$$

$$Q_{eg} = \dot{m}_{eg} c_{p,eg} (T_{eg,o} - T_{eg,i})$$

In the above equations, the air side surface temperature was first assumed by 1°C lower than the dew point and iterated to the condition when  $Q_{eg} = Q_{a,sen} + Q_{a,lat}$ .

### 3.3 Heat transfer rate for R1234yf

#### 3.3.1 Single phase HTC

When the Reynolds number is above 2300, Gnielinski's correlation [1] is used for determining Nusselt number:

$$Nu = \frac{f/8(Re - 1000)Pr}{1 + 12.7(f/8)^{1/2}(Pr^{2/3} - 1)}$$

$$f = [0.79 \ln(Re) - 1.64]^{-2}$$

When the Reynolds number is lower than 2300, Nusselt number is obtained by interpolation of data in Figure 3.


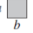
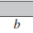
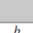
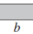
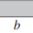
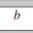
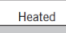


Cross Section	$\frac{b}{a}$	$Nu_D = \frac{HTC \cdot D_h}{k}$	
		(Uniform $q''_s$ )	(Uniform $T_s$ )
	—	4.36	3.66
	1.0	3.61	2.98
	1.43	3.73	3.08
	2.0	4.12	3.39
	3.0	4.79	3.96
	4.0	5.33	4.44
	8.0	6.49	5.60
	$\infty$	8.23	7.54
	$\infty$	5.39	4.86
	—	3.11	2.49

Figure 3. Laminar Flow Nusselt Number Table

#### 3.3.2 Two phase HTC

Kim's [4] correlation was adopted for heat transfer coefficient of two phase flow. The main equations for Kim's correlation is shown below:

$$h_{tp} = (h_{nb}^2 + h_{cb}^2)^{0.5}$$

$$h_{nb} = \left[ 2345 (Bo \frac{P_H}{P_F})^{0.70} P_R^{0.38} (1-x)^{-0.51} \right] (0.023 Re_f^{0.8} Pr_f^{0.4} \frac{k_f}{D_h})$$

$$h_{cb} = \left[ 5.2 (Bo \frac{P_H}{P_F})^{0.08} We_{fo}^{-0.54} + 3.5 \left( \frac{1}{X_{tt}} \right)^{0.94} \left( \frac{\rho_g}{\rho_f} \right)^{0.25} \right] (0.023 Re_f^{0.8} Pr_f^{0.4} \frac{k_f}{D_h})$$

where  $Bo = \frac{q''_H}{G h_{fg}}$ ,  $P_R = \frac{P}{P_{crit}}$ ,  $Re_f = \frac{G(1-x)D_h}{\mu_f}$ ,  $We_{fo} = \frac{G^2 D_h}{\rho_f \sigma}$ ,  $X_{tt} = \left( \frac{\mu_f}{\mu_g} \right)^{0.1} \left( \frac{1-x}{x} \right)^{0.9} \left( \frac{\rho_g}{\rho_f} \right)^{0.5}$ ,  
 $q''_H$ : effective heat flux averaged over heated perimeter of channel,  $P_H$ : heated perimeter of channel,  $P_F$ : wetted perimeter of channel

Kim also suggested a calculation for dry-out quality [6]. The correlation for dry-out quality is:

$$x_{di} = 1.4We_{fo}^{0.03}P_R^{0.08} - 15.0\left(Bo\frac{P_H}{P_F}\right)^{0.15}Ca^{0.35}\left(\frac{\rho_g}{\rho_f}\right)^{0.06}$$

$$\text{where } We_{fo} = \frac{G^2 D_h}{\rho_f \sigma}, P_R = \frac{P}{P_{crit}}, Bo = \frac{q_H''}{G h_{fg}}, Ca = \frac{\mu_f G}{\rho_f \sigma} = \frac{We_{fo}}{Re_{fo}},$$

$q_H''$ : effective heat flux averaged over heated perimeter of channel,

$P_H$ : heated perimeter of channel,  $P_F$ : wetted perimeter of channel

When the refrigerant quality is located between the dry-out quality and 1, linear interpolation was applied between the two-phase HTC and single-phase HTC.

### 3.4 Heat transfer rate for air

The air side heat transfer can be obtained with the correlation provided by Chang and Wang [2]:

$$htc_{air} = \rho_{air} \times Vel_{air} \times Cp_{air} \times St$$

$$St = j \times Pr_{air}^{-2/3}$$

$$j = Re_{Lp}^{-0.49} \left( \frac{\theta_{louver}}{90} \right)^{0.27} \left( \frac{P_{fin}}{P_{louver}} \right)^{-0.14} \left( \frac{h_{fin}}{P_{louver}} \right)^{-0.29} \left( \frac{D_{tube}}{P_{louver}} \right)^{-0.23} \\ \left( \frac{L_{louver}}{P_{louver}} \right)^{0.68} \left( \frac{P_{tube}}{P_{louver}} \right)^{-0.28} \left( \frac{t_{fin}}{P_{louver}} \right)^{-0.05}$$

### 3.5 Air side Hydraulic Performance

Air side pressure drop is calculated by the equation set provided by Chang and Wang [2]:

$$f = f_1 f_2 f_3$$

When  $Re_{Lp} < 150$ :

$$f_1 = 14.39 Re_{Lp}^{-0.805 \frac{P_{fin}}{D_{fin}}} \ln^{3.04} \left( 1 + \frac{P_{fin}}{P_{louver}} \right) \\ f_2 = \ln^{-1.435} \left( \left( \frac{t_{fin}}{P_{fin}} \right)^{0.48} + 0.9 \right) \left( \frac{D_{h,port}}{P_{louver}} \right)^{-3.01} \ln^{-3.01} (0.5 Re_{Lp}) \\ f_3 = \left( \frac{P_{fin}}{L_{louver}} \right)^{-0.308} \left( \frac{D_{fin}}{L_{louver}} \right)^{-0.308} \exp(-0.1167 \frac{P_{tube}}{h_{fin}}) \theta_{louver}^{0.35}$$

When  $150 < Re_{Lp} < 5000$ :

$$f_1 = 4.97 Re_{Lp}^{0.6049 - 1.064/\theta^{0.2}} (\ln((t_{fin}/P_{fin})^{0.5} + 0.9))^{-0.527} \\ f_2 = ((D_{h,port}/P_{louver}) \ln(0.3 Re_{Lp}))^{-2.966} (P_{fin}/L_{louver})^{-0.7931(P_{tube}/h_{fin})} \\ f_3 = (P_{tube}/t_{tube})^{-0.0446} (\ln(1.2 + (P_{louver}/P_{fin})^{1.4}))^{-3.553} \theta_{louver}^{-0.477}$$

The frictional factor  $f$  can also be expressed as:

$$f = \frac{A_c \rho_m}{A \rho_1} \left[ \frac{2 \rho_1 D P_{air}}{G_c^2} - (K_c + 1 - \sigma^2) - 2 \left( \frac{\rho_1}{\rho_2} - 1 \right) + (1 - \sigma^2 - K_e) \frac{\rho_1}{\rho_2} \right]$$

### 3.6 Refrigerant side Hydraulic Performance

#### 3.6.1 Single phase hydraulic performance

The pressure drop of EG is calculated by correlation provided by Churchill [3]:

$$DP_{ref} = DP_{ref,static} = \frac{\partial p}{\partial z} \frac{L_{elem}}{f D_{h,port}} \frac{G_{ref}^2}{2\rho_{ref}}$$

$$\frac{\partial p}{\partial z} = 8 \left( \left( \frac{8}{Re_D} \right)^{12} + \left( \frac{1}{A+B} \right)^{1.5} \right)^{\frac{1}{12}}$$

$$A = (-2.456 \ln^{0.9} \left( \frac{7}{Re_D} \right) + 0.27 \frac{Ra_{tube}}{D_{h,port}})^{16}$$

$$B = \left( \frac{37530}{Re_D} \right)^{16}$$

#### 3.6.2 Two phase hydraulic performance

The two-phase static pressure drops, Kim's [5] correlation is applied in the simulation for calculating the static pressure drop. The main equations are shown below:

$$\left( \frac{dp}{dz} \right)_F = \left( \frac{dp}{dz} \right)_f \phi_f^2$$

$$\text{where } \phi_f^2 = 1 + \frac{C}{X} + \frac{1}{X^2}, X^2 = \frac{(dp/dz)_f}{(dp/dz)_g}$$

$$-\left( \frac{dp}{dz} \right)_f = \frac{2f_f v_f G^2 (1-x)^2}{D_h}, -\left( \frac{dp}{dz} \right)_g = \frac{2f_g v_g G^2 x^2}{D_h}$$

$$f_k = 16 Re_k^{-1} \text{ for } Re_k < 2000$$

$$f_k = 0.079 Re_k^{-0.25} \text{ for } 2000 \leq Re_k < 20,000$$

$$f_k = 0.046 Re_k^{-0.2} \text{ for } Re_k \geq 20,000$$

for laminar flow in rectangular channel,

$$f_k Re_k = 24(1 - 1.3553\beta + 1.9467\beta^2 - 1.7012\beta^3 + 0.9564\beta^4 - 0.2537\beta^5)$$

where subscript  $k$  denotes  $f$  or  $g$  for liquid and vapor phases, respectively,

$$Re_f = \frac{G(1-x)D_h}{\mu_f}, Re_g = \frac{GxD_h}{\mu_g}, Re_{fo} = \frac{GD_h}{\mu_f}, Su_{go} = \frac{\rho_g \sigma D_h}{\mu_g^2}, We_{fo} = \frac{G^2 D_h}{\rho_f \sigma}, Bo = \frac{q_{H}''}{Gh_{fg}}$$

$$Re_f \geq 2000, Re_g \geq 2000 \text{ (tt)}$$

$$Re_f \geq 2000, Re_g < 2000 \text{ (tv)}$$

$$Re_f < 2000, Re_g \geq 2000 \text{ (vt)}$$

$$Re_f < 2000, Re_g < 2000 \text{ (vv)}$$

$$Re_f \geq 2000$$

$$Re_f < 2000$$

$C_{non-boiling}$

$$0.39 Re_{fo}^{0.03} Su_{go}^{0.10} \left( \frac{\rho_f}{\rho_g} \right)^{0.35}$$

$$8.7 \times 10^{-4} Re_{fo}^{0.17} Su_{go}^{0.50} \left( \frac{\rho_f}{\rho_g} \right)^{0.14}$$

$$0.0015 Re_{fo}^{0.59} Su_{go}^{0.19} \left( \frac{\rho_f}{\rho_g} \right)^{0.36}$$

$$3.5 \times 10^{-5} Re_{fo}^{0.44} Su_{go}^{0.50} \left( \frac{\rho_f}{\rho_g} \right)^{0.48}$$

$C$

$$C_{non-boiling} [1 + 60 We_{fo}^{0.32} (Bo \frac{P_H}{P_F})^{0.78}]$$

$$C_{non-boiling} [1 + 530 We_{fo}^{0.52} (Bo \frac{P_H}{P_F})^{1.09}]$$

## 4. Results and Discussion

### 4.1 Overall Performance of Cooling Coil

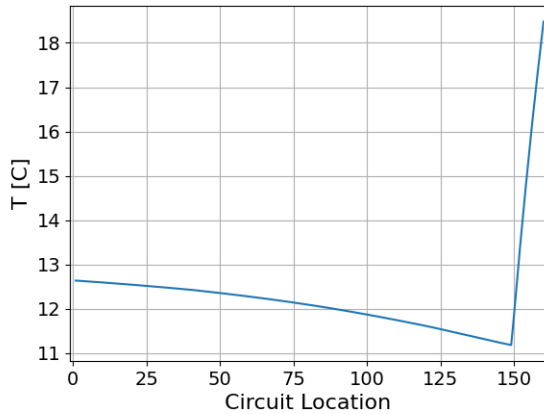
Figure 4 contains the plots of detailed overall performance of the cooling coil. The total performance of the cooling coil is presented in Table 4.

Table 4. Overall Performance

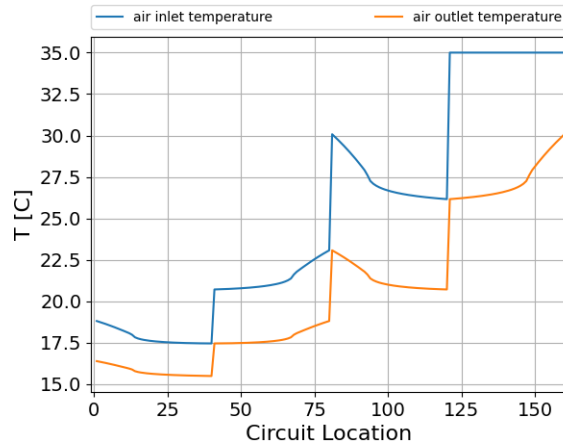
T_ero	T_eao	P_ero	Q_tot	Q_sen_tot	Q_lat_tot	SHR
19.03°C	15.76°C	451.78	4.32kW	2.94kW	1.37kW	68%

The following plot shows the profiles of some key parameters of interest. The plots are refrigerant across the evaporator flow path. Each slab has 40 segments, and in total there are 160 segments. For Figure 4(a), the refrigerant completely evaporated at 150 segment location. For the two-phase region, the refrigerant temperature started from 12.6°C and drops to 11.2°C due to the pressure drop of the refrigerant. For single-phase region, the refrigerant temperature increased sharply to 19.03°C. Figure 4(b) includes the air temperature inlet and outlet profile. Notice that for each adjacent pair of slabs, the inlet air temperature and outlet temperature are symmetric due to the design of the evaporator. The air flows into the evaporator at the 4<sup>th</sup> slab with 35°C temperature, and leaves the evaporator at the 1<sup>st</sup> slab with around 15.8°C temperature. And as R1234yf evaporated through the microchannels, the temperature difference between the air inlet and outlet temperature decreased. The air outlet dew point temperature, sensible heat transfer rate and latent heat transfer rate are shown in Figure 4(c), (g) and (h). As the air enters evaporator, at the location very close to the outlet of the evaporator, there was no water condensation due to high temperature of R1234yf. When the temperature of R1234yf is slightly lower, the latent heat transfer rate increases up to 0.6W per segment. However, since the water vapor in the air flow decreases and the air becomes dryer, the latent heat transfer rate starts to decrease and ends at around 0.25W per segment. The R1234yf heat transfer coefficient profile is shown in Figure 4(e). When R1234yf starts to evaporate, the velocity of the refrigerant increases which leads to the increase of HTC from  $1600 \text{ W/m}^2\text{K}$  to  $2300 \text{ W/m}^2\text{K}$ . However, after the vapor quality of R1234yf passes the dry-out quality, the HTC starts to decrease, and resulted in single phase HTC which is around  $700 \text{ W/m}^2\text{K}$ . From Figure 4(f), the evaporator has best heat transfer performance at 3<sup>rd</sup> slab and the first half of 4<sup>th</sup> slab. At the first two slabs, the temperature difference between R1234yf and the air is smaller compared to 3<sup>rd</sup> and 4<sup>th</sup> slab. While at the later half of the 4<sup>th</sup> slab, R1234yf fully evaporated, which leads to the decrease of heat transfer rate (drops from 1.8W per segment to 0.8W per segment).

(a) R1234yf Temperature



(b) Air Temperature



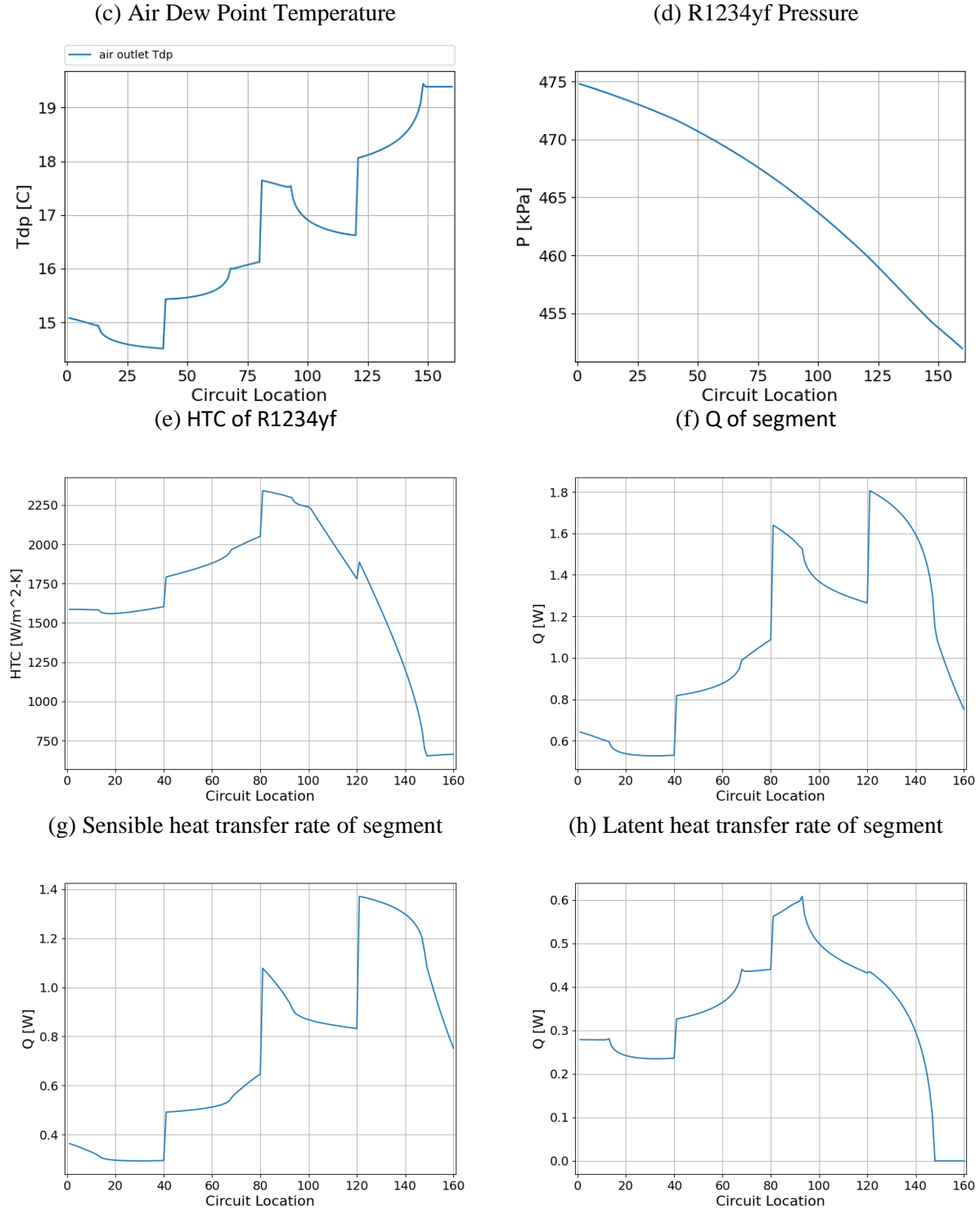


Figure 4. Overall Performance of cooling coil. (a) EG temperature distribution; (b) Air inlet and outlet dry bulb temperature; (c) air inlet and outlet dew point temperature; (d) EG pressure distribution; (e) EG heat transfer coefficient distribution; (f) Total heat transfer rate in each segment; (g) sensible heat transfer rate in each segment; (h) latent heat transfer rate in each segment.



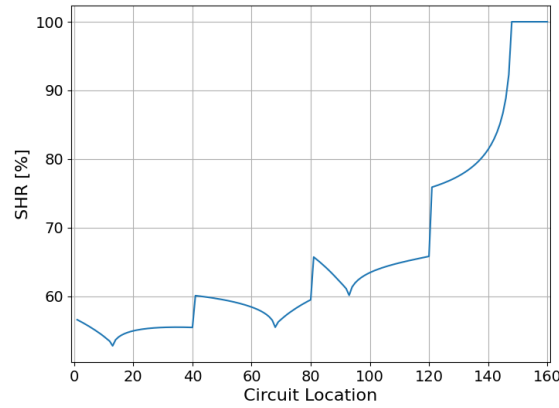


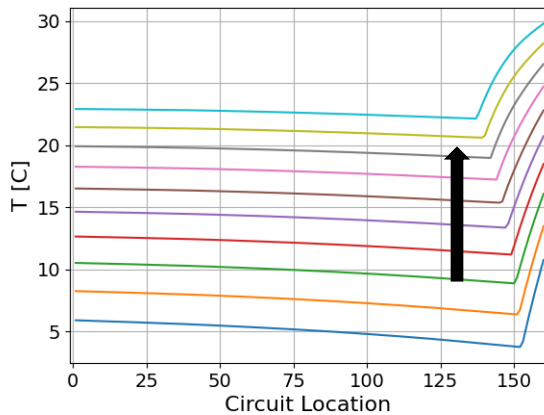
Figure 5. Overall SHR of Evaporator

Figure 5 shows the SHR of each segment. As refrigerant flows through the slabs, the SHR of each slab gradually increases, and at the 4<sup>th</sup> slab, the SHR reaches 100% at the location close to the outlet of the evaporator. The SHR in the first 3 slabs are very close, around 60%. The sudden increase of SHR in the 4<sup>th</sup> slab is because R1234yf becomes superheated vapor.

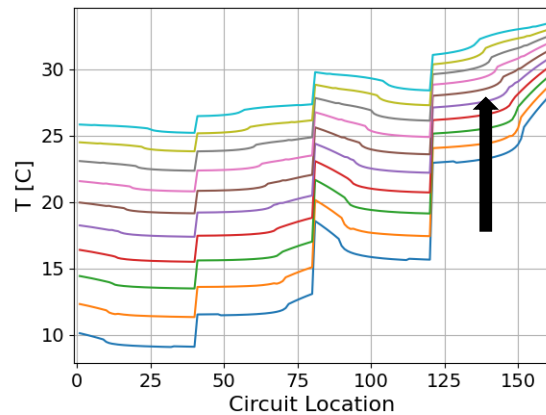
#### 4.2 Impact of Relative Humidity

To analyze the impact of relative humidity, performance of evaporator was plotted with relative humidity ranges from 0.2 to 0.8. The arrow direction indicates the increasing relative humidity. For higher relative humidity of air inlet conditions, the refrigerant inlet and outlet temperatures are higher in order to meet the superheated level requirement. The refrigerant inlet temperature increases from 5.9°C to 22.9°C, and the refrigerant outlet temperature increases from 11.6°C to 30.0°C. Since the refrigerant temperature and pressure are correlated, in Figure 6(d), as relative humidity increases, the pressure of R1234yf increases from 375kPa to 625kPa. Since the refrigerant temperature increases with the increase of relative humidity ratio, the temperature difference between R1234yf temperature and air inlet temperature reduces, which leads to the increase of outlet air temperature from 9.33°C to 25.54°C.

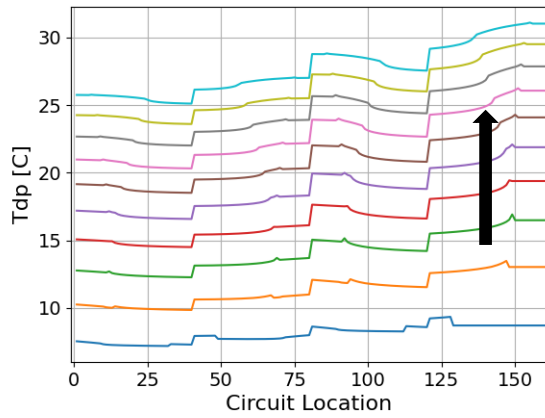
(a) R1234yf Temperature



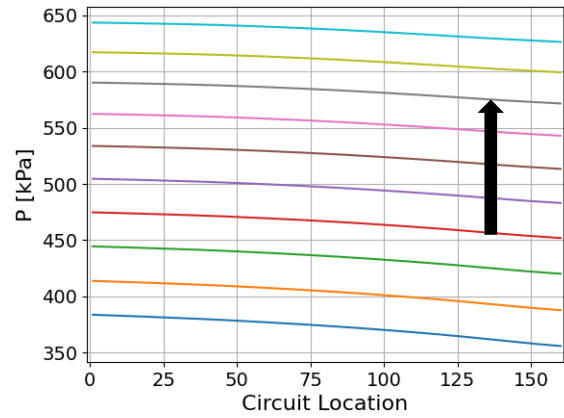
(b) Air Outlet Temperature



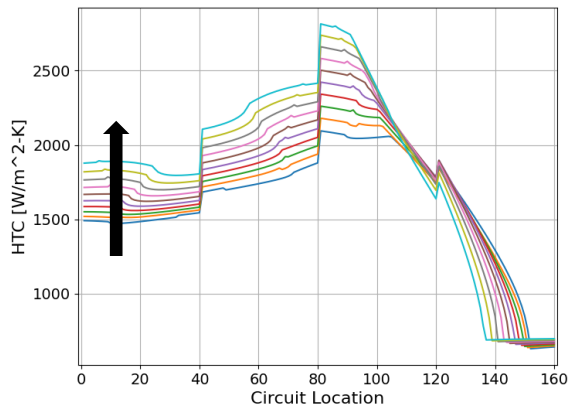
c) Air Outlet Dew Point Temperature



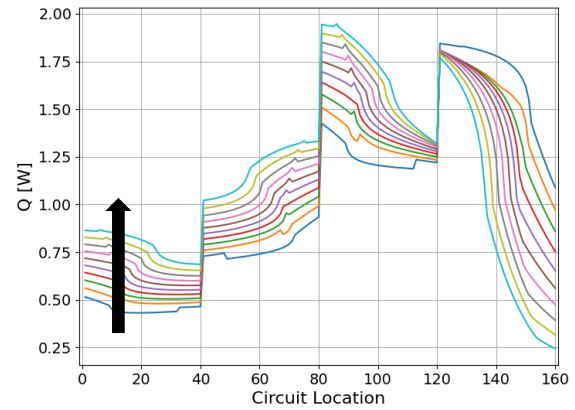
(d) R1234yf Pressure



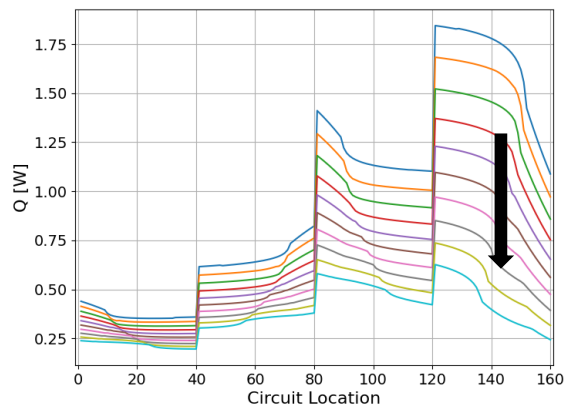
(e) HTC of R1234yf



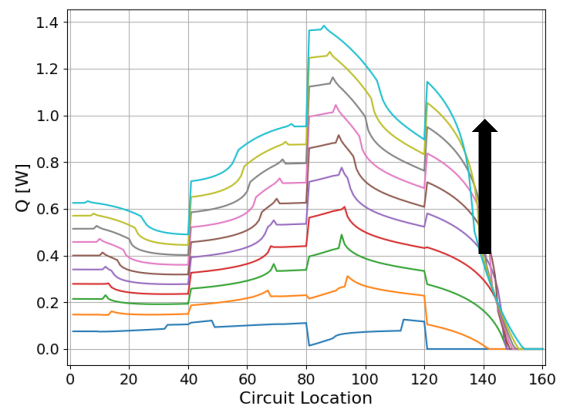
(f) Heat transfer rate of each segment



(g) Sensible heat transfer rate of each segment



(h) Latent heat transfer rate of each segment



(i) SHR of each segment

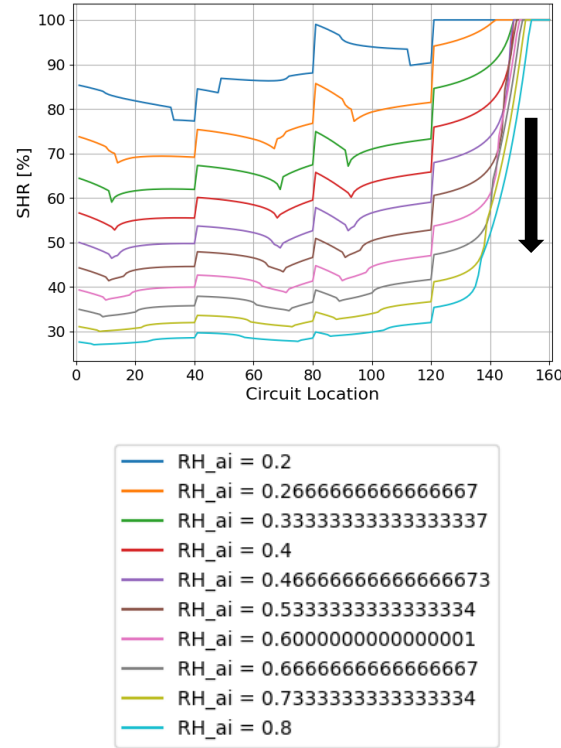


Figure 6. Impact of relative humidity on the performance of cooling coil. (a) EG Temperature; (b) Air outlet temperature; (c) air outlet dew point temperature; (d) EG pressure; (e) EG heat transfer coefficient; (f) segment heat transfer rate; (g) segment sensible heat transfer rate; (h) segment latent heat transfer rate; (i) SHR of each segment.

With higher relative humidity, the air inlet dew point temperature increases from 8.3°C to 28.5°C. Higher dew point temperature leads to more water condensation, which can be reflected from Figure 6(h). For higher relative humidity, latent heat transfer rate of the evaporator increases from 0.26kW to 3.08kW. Meanwhile, the sensible heat transfer rate decreases from 3.88kW to 1.49kW. But the total heat transfer rate increases slightly from 4.14kW to 4.57kW. Thus, increasing the relative humidity can improve the total heat transfer rate of the evaporator.

## 5. Conclusions

The heat transfer and hydraulic performance of an evaporator was simulated with python and package CoolProp. The simplified condensation model is applied for the condition that surface temperature is lower than the dew point temperature. The overall performance and parameters of interest were shown. Impacts of relative humidity and air volumetric flow rate were investigated and compared. When increasing the relative humidity, the sensible heat transfer rate decreased while the latent heat transfer rate increased; and the total heat transfer rate of the evaporator increased by 10%.

## 6. References

- [1] Gnielinski, Volker. "New equations for heat and mass transfer in the turbulent flow in pipes and channels." NASA STI/recon technical report A 41.1 (1975): 8-16.
- [2] Chang, Y-JY-J., et al. "A generalized friction correlation for louver fin geometry." *International journal of heat and mass transfer* 43.12 (2000): 2237-2243.
- [3] Churchill, Stuart W. "Friction-factor equation spans all fluid-flow regimes." (1977).
- [4] Kim, Sung-Min, and Issam Mudawar. "Universal approach to predicting two-phase frictional pressure drop for mini/micro-channel saturated flow boiling." *International Journal of Heat and Mass Transfer* 58.1-2 (2013): 718-734.
- [5] Kim, Sung-Min, and Issam Mudawar. "Universal approach to predicting saturated flow boiling heat transfer in mini/micro-channels—Part II. Two-phase heat transfer coefficient." *International Journal of Heat and Mass Transfer* 64 (2013): 1239-1256.
- [6] Kim, Sung-Min, and Issam Mudawar. "Universal approach to predicting saturated flow boiling heat transfer in mini/micro-channels—Part I. Dryout incipience quality." *International Journal of Heat and Mass Transfer* 64 (2013): 1226-1238.